COMMUNICATION

Hexagonal Boron Nitride

ADVANCED
MATERIALS
INTERFACES

www.advmatinterfaces.de

Direct Growth of 5 in. Uniform Hexagonal Boron Nitride on Glass for High-Performance Deep-Ultraviolet Light-Emitting Diodes

Qiucheng Li, Qingqing Wu, Jing Gao, Tongbo Wei, Jingyu Sun, Hao Hong, Zhipeng Dou, Zhepeng Zhang, Mark H. Rümmeli, Peng Gao, Jianchang Yan,* Junxi Wang, Jinmin Li, Yanfeng Zhang,* and Zhongfan Liu*

The direct coating of 2D hexagonal boron nitride (h-BN) on insulating solid glass will endow glass with advanced properties, thus offering killer applications of the new type hybrid of h-BN glass. However, daunting challenges still remain regarding the direct growth methodology of h-BN on glass. Herein, a catalyst-free chemical vapor deposition route for the direct synthesis of 5 in. uniform h-BN thin films on functional quartz and sapphire glass is developed. The optical transparency, surface wetting, and thermal conductivity of glass are readily tailored by varying the deposited h-BN thicknesses from monolayer to over 20 layers. Encouragingly, the as-obtained h-BN/sapphire glass can serve as a stress-releasing substrate for the van-der-Waals epitaxial growth of AlN functional layers, as well as a thermal conductive template for constructing high-performance deep-ultraviolet light-emitting diodes. This work hereby provides a brand new direction for the application of h-BN glass in next-generation solid-state lighting devices.

Hexagonal boron nitride (h-BN) is a III–V compound possessing a similar honeycomb lattice structure to graphene, but with a considerable bandgap energy (≈5.8 eV).[1] Such a graphene analogue has drawn intensive attentions in recent years due to its high thermal conductivity (2000 W m^{-1} K^{-1}),[2] large mechanical strength (Young's modulus ≈ 1.16 TPa),[3] superior optical transparency,[1] chemical stability (up to 1100 °C),[4] and atomically flat surface.[5] Numerous applications have been developed accordingly, such as far-ultraviolet light-emitting devices,[1] oxidation-resistant coatings,[4,6] transparent electronics,[7] thermal conductive systems,[8,9] etc. Particularly, the integration of graphene with h-BN (as dielectric substrates) has simulated widespread research interests in constructing high-performance field-effect transistors[10,11] and exploring fundamental issues in condensed matter physics.[12,13]

Chemical vapor deposition (CVD) has been widely adopted for the direct synthesis of monolayer or thin-layer h-BN films, mainly on various metal substrates (e.g., Cu,[14] Ni,[15] Pt,[16] Fe,[3] Cu-Ni alloys[17]). However, most of the applications for such CVD-derived h-BN layers are inevitably involved with a tedious transfer process

Dr. Q. C. Li, H. Hong, Z. P. Dou, Z. P. Zhang, Prof. P. Gao,
Prof. Y. F. Zhang, Prof. Z. F. Liu
Center for Nanochemistry (CNC)
Beijing Science and Engineering Center for Nanocarbons
Beijing National Laboratory for Molecular Sciences
College of Chemistry and Molecular Engineering
Peking University
Beijing 100871, China
E-mail: yanfengzhang@pku.edu.cn; zfliu@pku.edu.cn
Dr. Q. C. Li, Dr. J. Gao, Prof. J. Y. Sun, Prof. M. H. Rümmeli, Prof. Z. F. Liu
Soochow Institute for Energy and Materials InnovationS (SIEMIS)
Key Laboratory of Advanced Carbon Materials and Wearable Energy
Technologies of Jiangsu Province
Soochow University
Suzhou 215006, China
Q. Q. Wu, Prof. T. B. Wei, Prof. J. C. Yan, Prof. J. X. Wang, Prof. J. M. Li
Research and Development Center for Solid State Lighting
Institute of Semiconductors
Chinese Academy of Sciences
Beijing 100083, China
E-mail: yanjc@semi.ac.cn

Q. Q. Wu, Prof. T. B. Wei, Prof. J. C. Yan, Prof. J. X. Wang, Prof. J. M. Li
University of Chinese Academy of Sciences
Beijing 100049, China
Z. P. Dou, Prof. P. Gao
Electron Microscopy Laboratory, and International
Center for Quantum Materials
School of Physics
Peking University
Beijing 100871, China
Z. P. Dou, Prof. P. Gao
Electron Microscopy Laboratory
Collaborative Innovation Center of Quantum Matter
Beijing 100871, China
Prof. Y. F. Zhang, Prof. Z. F. Liu
Beijing Graphene Institute (BGI)
Beijing 100095, P. R. China

from growth substrates to target (mostly insulating) substrates. This multistep transfer would normally degrade the quality of h-BN layers because of the formation of tears, folds, wrinkles, and the adsorption of polymeric impurities.[18] More significantly, the metals consumption and environmental pollution is always accompanied.[19]

To further extend the practicability of h-BN, combining 2D h-BN with some functional substrates is highly desired. Various types of glass (i.e., quartz, sapphire, soda-lime glass) have been developed as templates for the direct CVD synthesis of graphene, affording a novel hybrid material of graphene glass with intriguing applications, such as transparent electrodes, smart windows, low-cost heating devices.[20–22] Notably, the direct CVD synthetic route is also applicable to the growth of h-BN on insulating glass substrates. As reported previously, although lack of metal catalysts, h-BN still nucleated at the oxygen dangling bonds of quartz or SiO_2 surfaces,[23] and can be epitaxially grown on sapphire substrates.[24–26]

The direct coating of h-BN on large-scale quartz or sapphire glass is promising for the direct fabrication of all-transparent optoelectronic devices, such as III-nitride-based (e.g., GaN, AlGaN, InGaN) light-emitting diodes (LEDs).[27,28] In general, III-nitride-based films were grown on sapphire substrates, which would cause mediocre device performances due to the poor thermal conductivity of sapphire and the severe interface stress built from the large lattice mismatch of adlayer/sapphire.[28] The accumulated stress within the III-nitride epilayers usually deteriorates the crystalline quality of the epilayers, and brings huge challenges during the device fabrication process. Encouragingly, h-BN possesses the similar honeycomb structure and atomic flat surface, making it a perfect buffer layer for the heteroepitaxy of nitride semiconductors.

This template is also reliable for overcoming the thermal issues under high driving currents in LEDs, which is similar to the case of embedded graphene oxide in a GaN-based LED with improved device performances and good durability.[29] Moreover, the weak van-der-Waals (vdW) interaction between the adlayer and h-BN could enable the mechanical transfer of LED devices onto foreign substrates.[27,30]

In the present work, we have accomplished the direct CVD growth of h-BN thin films on functional quartz and sapphire glass, by using an optimized low-pressure (LP) CVD route. 5 in. uniform, thickness tunable, high-quality h-BN films have been achieved directly on glass, offering a new type of hybrid material of h-BN glass. Intriguingly, the as-obtained h-BN glass exhibited excellent optical transparency, ultraflat surface, good thermal conductivity, etc. The new type hybrid material of h-BN on sapphire glass was also utilized as a perfect candidate for the direct epitaxial growth of III-nitride semiconducting films, for the fabrication of high-performance deep-ultraviolet (DUV) LED devices.

Figure 1a illustrates the schematic diagram of the LPCVD growth process for achieving h-BN thin films on a solid glass surface. Herein, representative types of solid glass (i.e., quartz and sapphire) were selected as growth substrates, considering their high melting points and relatively flat surfaces (Figure S1, Supporting Information). Typically, the h-BN growth was performed with the substrate held at 1100 °C in a three-zone furnace, by using vaporized ammonia boron (NH_3BH_3) as precursor. Systematic parameter investigations have revealed that, the evaporation temperature of the solid NH_3BH_3 precursor (T_P) and the growth time (t) were the key parameters for h-BN growth (with more details described in the Experimental Section).
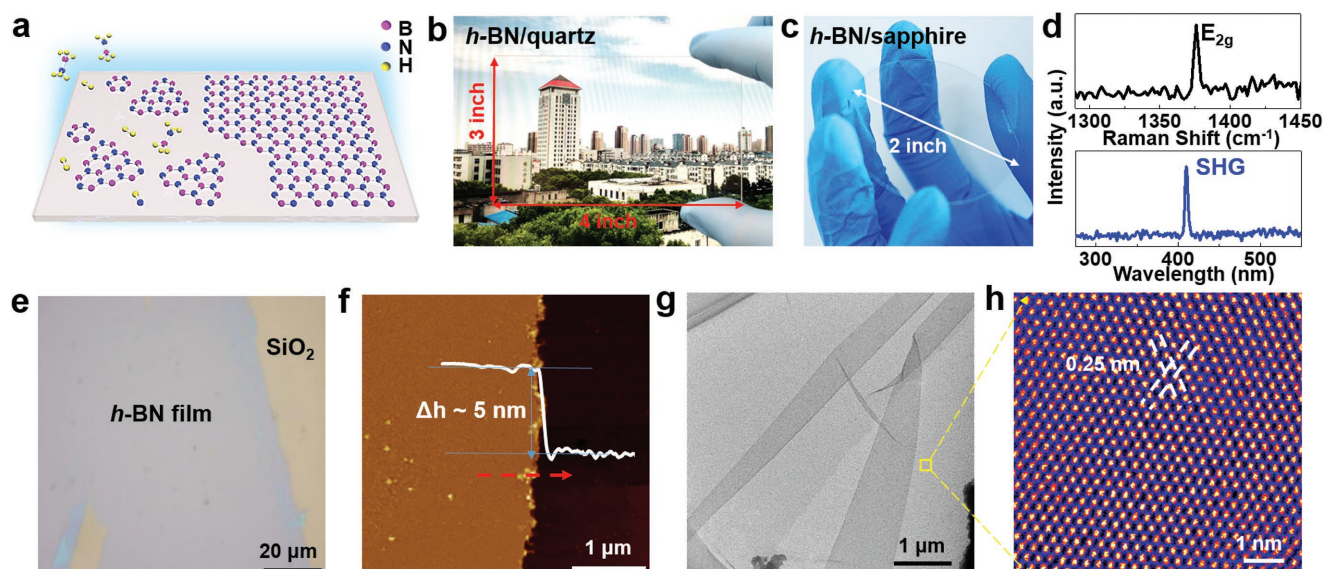

Figure 1. LPCVD growth of large-area uniform h-BN films on quartz and sapphire glass. a) Schematic diagram of the initial CVD growth process. b) Photograph of a 4 in. × 3 in. uniform h-BN film grown on quartz glass showing a rather high transparency with regard to the underneath picture. c) Photograph of a 2 in. uniform h-BN film synthesized on a sapphire wafer. d) Corresponding Raman (upper panel) and SHG (lower panel) spectra of the as-achieved h-BN film on quartz glass revealing its relative high crystal quality. e) Typical OM image of the transferred h-BN film on SiO_2/Si. f) AFM image of the transferred film showing a thickness of ≈5 nm and a roughness of ≈0.11 nm, respectively. g,h) Low-magnification and atomic-resolution TEM images of a transferred h-BN film on the TEM Cu grid. The growth conditions of the samples (evaporation temperature of BH_3-NH_3 precursor (T_P) and growth time (t)): (b, c, d, e, f) T_P = 85 °C, t = 1 h ; (g, h) T_P = 80 °C, t = 1 h with the substrates held at 1100 °C under Ar and H_2 carrier gases.

**ADVANCED
SCIENCE NEWS**
www.advancedsciencenews.com

**ADVANCED
MATERIALS
INTERFACES**
www.advmatinterfaces.de

After LPCVD growth processes, the quartz glass (5 in. for the diagonal length) and sapphire wafer (2 in. in diameter) demonstrate highly uniform, transparent features over the whole samples, as presented by the photographs in Figure 1b,c, respectively. The direct coating of h-BN layers on both types of glass was confirmed by Raman spectroscopic characterizations, presenting a typical E_{2g} phonon mode centered at 1374 cm^{-1} (upper panel in Figure 1d). Besides, second-harmonic generation (SHG) at 410 nm was also acquired (lower panel in Figure 1d) under a pulse laser excitation (820 nm, 100 fs) to serve as an additional evidence for the successful formation of h-BN, due to the broken inversion symmetry of h-BN with an odd layer thickness.[31]

The formation of uniform h-BN films was further justified by a sample transfer process onto the SiO$_2$/Si substrate or the Cu grid for further characterizations, where the quartz substrates were etched away with the dilute HF aqueous solution (sapphire was etched away with the hot NaOH aqueous solution). In the optical microscope (OM) image of the transferred sample, a highly uniform color contrast was noticeable to address the relative high thickness uniformity of h-BN (Figure 1e). Corresponding atomic force microscope (AFM) image in Figure 1f demonstrates a film thickness of ≈5 nm, as well as an atomically flat surface (Ra ≈ 0.11 nm) with regards to the SiO$_2$/Si substrate. More AFM images of h-BN films with different thicknesses are displayed in Figure S2 (Supporting Information).

To attain a detailed structural inspection of the h-BN film, aberration-corrected, high-resolution transmittance electronic microscope (HRTEM) characterizations were employed on thin-layer h-BN sample. The low-magnified TEM view in Figure 1g indicates the existence of a highly continuous h-BN film on the TEM grid. Corresponding high-magnified TEM image (Figure 1f) reveals a honeycomb structure with an inter-atomic distance of ≈0.25 nm, in good agreement with that of bulk h-BN.[14] Moreover, X-ray photoelectron spectroscopy (XPS) (Figure S3, Supporting Information) data of the as-grown sample show highly symmetric B 1s and N 1s peaks at 190.8 and 398.4 eV, respectively, indeed suggesting the sp^2-hybridized feature.[25] According to the abovementioned results, it can be inferred that, highly uniform h-BN films can be successfully synthesized on solid glass by using a metal-free LPCVD route. The sample size can be scalable up to 5 in., which is only limited by the size of the CVD furnace.

It is reasonable to find that, the thicknesses of the h-BN films can be comprehensively tailored by varying the precursor feeding rate. **Figure 2**a shows photographs of bare quartz glass substrates (leftmost, as reference) and the h-BN/quartz glass samples grown by exposing the substrates to different T_p (75, 80, and 85 °C, respectively) heated BH$_3$-NH$_3$ precursors for 1 h (the other three samples). Notably, after the LPCVD growth process, the quartz glass templates present almost the same color contrast with that of pure quartz, highly indicative of the visible light transparent feature of the h-BN
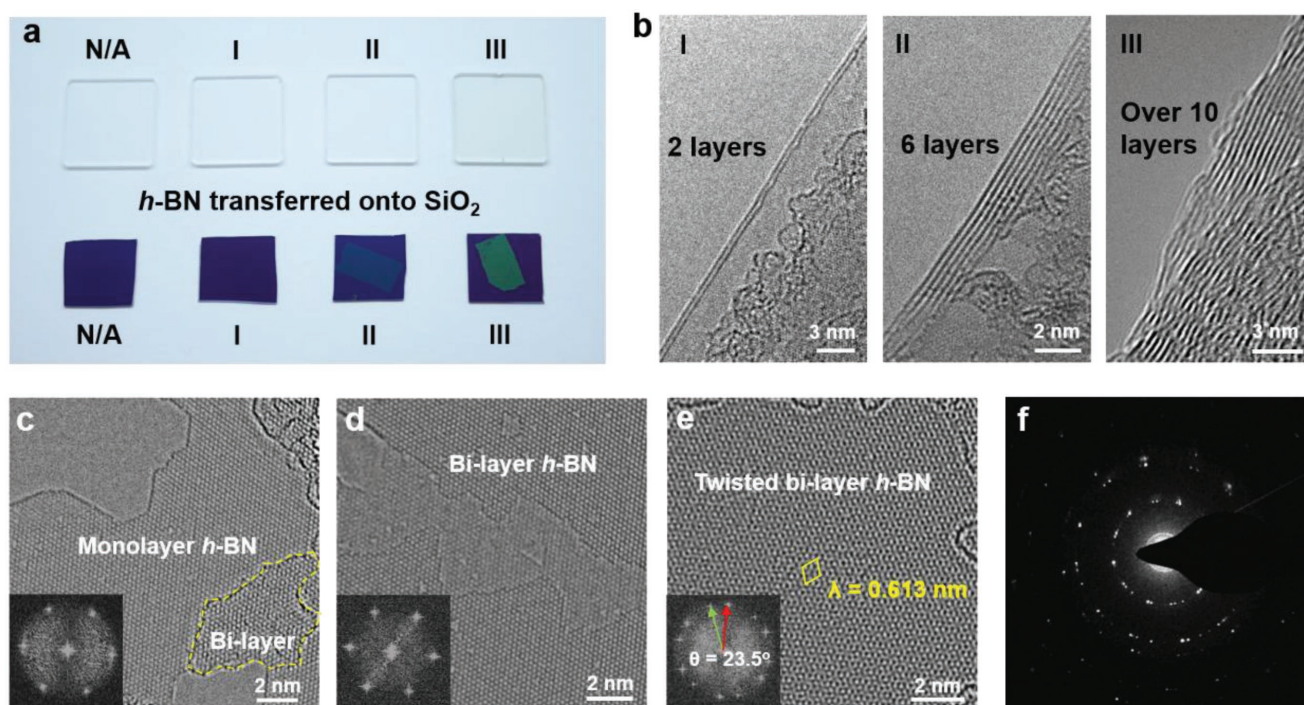
Figure 2. TEM characterizations of thickness tunable h-BN films. a) Photographs of the h-BN/quartz samples, marked from I to III achieved through exposing substrates to 75, 80, and 85 °C heated BH$_3$-NH$_3$ precursor for 1 h, respectively. The h-BN glass samples present almost the same color contrast with that of bare quartz, while the corresponding contrasts of the transferred h-BN on SiO$_2$/Si varies from nearly invisible (I), blue (II) to turquoise (III), correspondingly. b) TEM sectional views of the h-BN films obtained from samples I, II, III, revealing average film thicknesses of ≈2, ≈6, and over 10 layers, respectively. c) Representative HRTEM image showing mixed mono- and bilayer h-BN regions for sample I. d,e) HRTEM images of bilayer h-BN films showing the dominant A-A stacking registry and the twisted stacking geometry with the formation of moiré pattern, respectively. f) SAED pattern revealing a polycrystalline nature of the h-BN film.

ADVANCED
SCIENCE NEWS
www.advancedsciencenews.com

ADVANCED
MATERIALS
INTERFACES
www.advmatinterfaces.de

films. The h-BN thicknesses were estimated to be variable from monolayer to ≈20 layers, as evidenced by their distinct optical contrasts after being transferred onto SiO_2/Si substrates (lower panel in Figure 2a). Specifically, thin-layer h-BN (sample I) were obtained with T_p setting at 75 °C, as defined by its identical purple contrast with the bare SiO_2/Si. Multilayer h-BN films were attained by varying T_p from 80 to 85 °C, respectively, showing obvious contrast changes from blue (sample II) to turquoise (sample III). The detailed layer thicknesses were further probed with the aid of HRTEM sectional views. Three representative thicknesses of 2, 6, and over 10 layers are presented in Figure 2b, in line with sample I, II, and III, respectively.

Moreover, for the h-BN films grown on sapphire, a predominant epitaxial growth mode was observed with the h-BN domains showing a uniform orientation, which is different from the random orientations of h-BN films grown on quartz (as shown in Figure S4, Supporting Information). The HRTEM image in Figure 2c reveals the perfect atomic lattices of thin-layer h-BN with a mixed mono- and bilayer region (marked with yellow circle). The lattice orientation in each region is almost identical, affording an A-A stacking geometry in the bilayer region (Figure 2c). Some triangle shape breakages or blank holes, induced by the e-beam irradiation, also appear in the bilayer regions, which allow us to confirm the bilayer nature of the h-BN film (Figure 2d). On the other hand, twisted bilayer h-BN region with a moiré period of ≈0.613 nm is also observed with a 23.5° rotational angle, in consistent with the fast Fourier transform (FFT) pattern (Figure S5, Supporting Information). To better understand its stacking registry, a statistical analysis of the relative rotation angles of h-BN films (derived from 75 domains) is displayed in Figure S6 (Supporting Information), presenting a dominant A-A stacking geometry in the CVD-derived h-BN films.
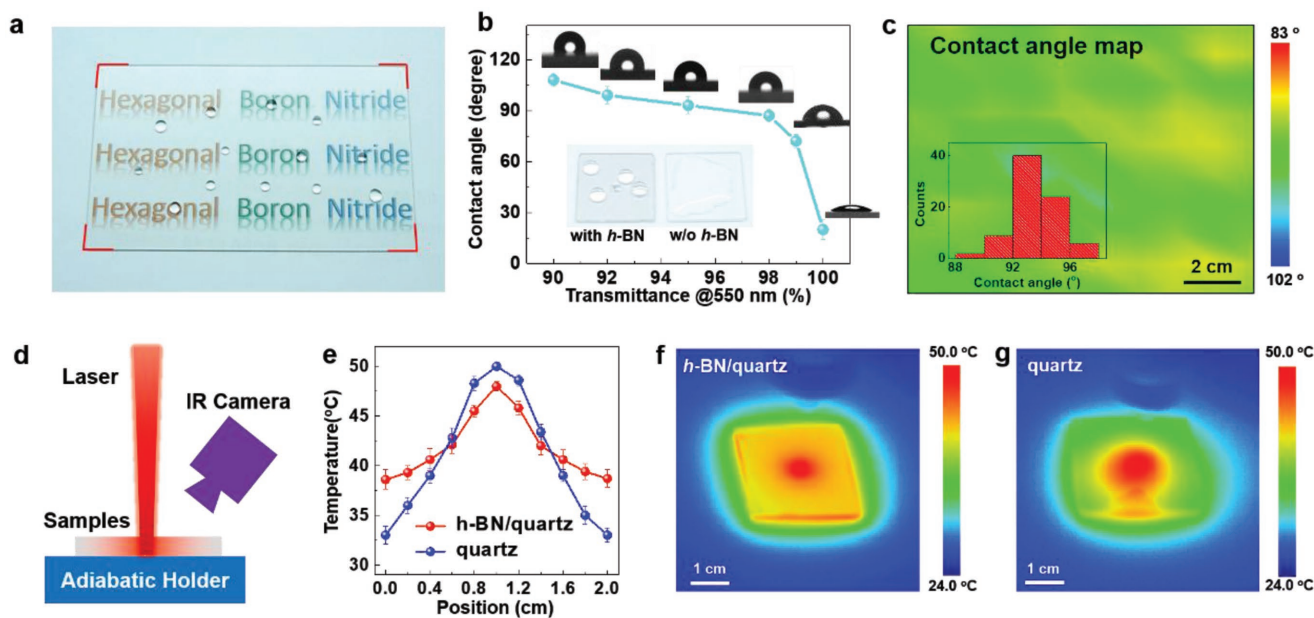
The crystalline quality of the as-obtained h-BN films was further confirmed by selected-area electron diffraction (SAED) patterns, showing several sets of sixfold-symmetric spots (Figure 2f). The average domain size of the as-achieved h-BN film is in the range from several tens of nanometers to several hundred nanometers (determined by dark-field TEM characterizations, as shown in Figure S7, Supporting Information), comparable with that of directly synthesized graphene on insulating substrates.[20,21] These characterizations again verify that highly uniform, thickness tunable, high-quality h-BN films can be successfully synthesized on high melting point glass following a metal-catalyst-free growth mechanism.

The optical performances of h-BN glass were systematically studied through direct comparisons of h-BN/quartz and graphene/quartz glass samples with comparable thicknesses (**Figure 3**a, with bare quartz serving as a reference). Evidently, the h-BN glass exhibits good transparency even with ≈20 layer h-BN coating (leftmost, marked with red box), which is markedly distinguished from the opaqueness displayed for graphene glass. This optical performance disparity is essentially determined by the different energy band structures of h-BN and graphene. The ultraviolet–visible (UV–vis) absorption spectrum of monolayer h-BN clearly shows one absorption edge at ≈200 nm (inset of Figure 3b), corresponding to an optical bandgap of ≈5.8 eV derived by the Tauc's equation (Figure 3b). Additional UV–vis absorption measurements of thin-layer h-BN samples were also performed (Figure S8, Supporting Information), implying similar band structures. Accordingly, the visible light absorption in h-BN glass is almost negligible due to its large bandgap.

For more details, the optical transmittances at 550 nm (T_{550}) were measured to be ≈99% for monolayer, ≈96% for 6–10 layers, and ≈90% for over 20 layers h-BN films (Figure 3c),
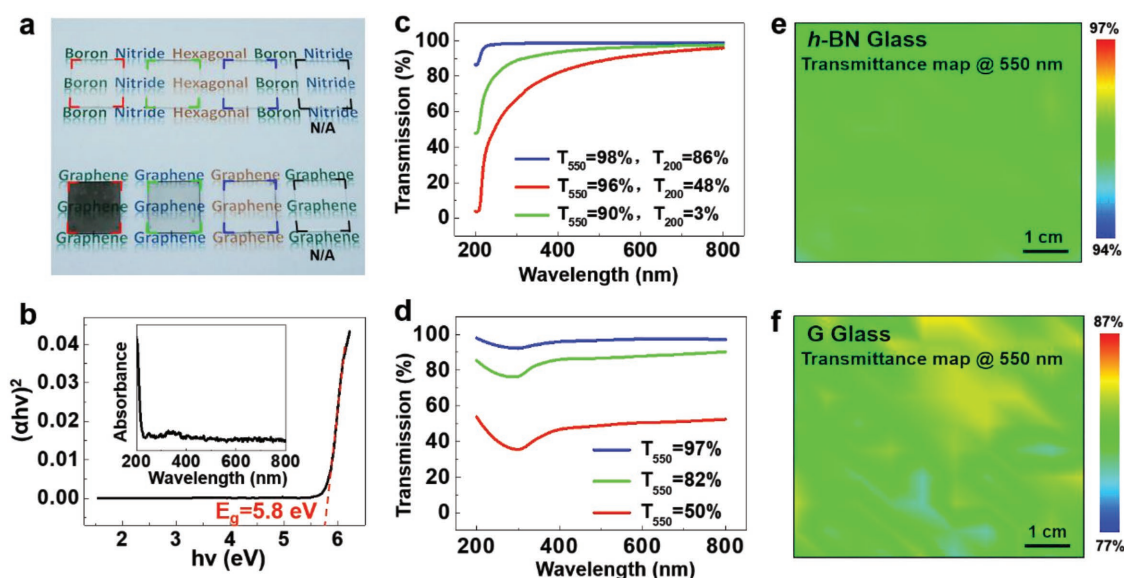
Figure 3. Excellent optical performances of h-BN glass. a) Photograph of h-BN/quartz and graphene/quartz samples with thicknesses of 1–2 layers (blue box), 6–10 layers (green box), and over 20 layers (red box), respectively. b) UV–vis absorbance spectrum (inset) and Tauc plot showing an optical bandgap of ≈5.8 eV for monolayer h-BN. c,d) Corresponding transmittance spectra of the h-BN/quartz and graphene/quartz samples marked in (a), respectively. e) Spatial distribution of the transmittance of h-BN layers @ 550 nm (6–10 layers, T_P ≈ 80 °C, 1 h). d) Spatial distribution of the transmittance of graphene glass @ 550 nm (6–10 layers, 5 vol% CH_4, 2 h).

**ADVANCED
SCIENCE NEWS**
www.advancedsciencenews.com

**ADVANCED
MATERIALS
INTERFACES**
www.advmatinterfaces.de

Figure 4. Surface characteristics of a large-scale uniform h-BN glass. a) Photograph of a 10 cm × 6 cm h-BN/sapphire glass synthesized with $T_p \approx 80$ °C for 1 h, displaying good visible light transparency. b) Water contact angle (θ) plotted as a function of transmittance at 550 nm (T_{550}) for various h-BN/quartz samples ($\theta = 108°$ for $T_{550} = 90\%$; $\theta = 99°$ for $T_{550} = 92\%$; $\theta = 93°$ for $T_{550} = 95\%$; $\theta = 89°$ for $T_{550} = 98\%$; $\theta = 72°$ for $T_{550} = 99\%$). The inset images show the hydrophobic and hydrophilic characteristics of the h-BN glass (left, $T_{550} = 90\%$) and bare glass (right), respectively. c) Corresponding spatial distribution of water contact angle for the h-BN glass ($\theta = 93°$ for $T_{550} = 95\%$; inset: statistical distribution of the contact angle). d) Schematic illustration of the temperature distribution map when applying a hot spot by a focused laser beam. e) Temperature plots and temperature distribution images of f) h-BN coated quartz and g) pristine quartz, respectively.

respectively. In contrast, the visible light absorption per graphene layer is ≈2.3%,[32] inevitably causing marked transparency degradation of graphene layers with similar thicknesses (from ≈97, 86, to ≈50% at 550 nm, as shown in Figure 3d). The large-scale uniformity of the transparencies for the h-BN glass and graphene glass samples (with identical thickness of ≈6–10 layers) was further mapped out at a 6 cm × 5 cm scale. Evidently, the h-BN glass displays a uniform transmittance of ≈96% at 550 nm (Figure 3e), in stark contrast to the inhomogeneous transmittance distribution of graphene glass from ≈80.5 to ≈84.4% at 550 nm (Figure 3f). In this regard, the h-BN glass with remarkably uniform optical transparency should be promising for various applications in transparent electronics and optoelectronics.

In addition to the excellent transparency, the surface feature of h-BN glass is indeed crucial for engineering its killer applications. h-BN is known as a hydrophobic and thermal conductive material, complementary to that of traditional glass.[33] In this work, the surface hydrophobicity of h-BN glass was characterized with a 10 cm × 6 cm h-BN glass sample with ≈96% transmittance at 550 nm (**Figure 4**a). The water dropping test revealed that, the water droplets can stay still on the h-BN glass, in sharp contrast to the film-wise formation of water on bare glass. Static contact angle measurement has shown a clear disparity between h-BN glass (>72°) and bare glass (≈20°). Moreover, the contact angle of h-BN glass was increased accordingly with increasing the layer thickness of h-BN (Figure 4b), varying from ≈72° (monolayer h-BN, ≈99% transmittance at 550 nm) to ≈108° (over 20 layers, ≈90% transmittance at 550 nm). This phenomenon is in accordance with the results obtained in

graphene glass,[22] which is possibly induced by the surface imperfections of grain boundaries and cracks.

To further address the large-scale uniformity of the hydrophobicity, the contact angle mapping was also conducted (Figure 4c), showing a narrow range of 89°–97°. The contact angle values were also compared with other reported results (Figure S9, Supporting Information), and our CVD-grown h-BN on glass demonstrated competitive hydrophobicity to other CVD-grown flat h-BN layers. This is possibly due to the wrinkle-free surface of h-BN directly grown on quartz and sapphire glass,[23,24] as distinguished from the h-BN films grown on metals with ubiquitous wrinkles that usually introduced vertical dipoles and thus significantly decreased surface hydrophobicity.[33,34] Consequently, the direct coating of h-BN on glass is effective in tailoring the surface hydrophobicity of glass, which may be utilized to fabricate self-cleaning glass with an ultrahigh transparency.

h-BN is known as a perfect heat conductive material with a theoretical thermal conductivity of ≈2000 W m^{-1} K^{-1}.[2] To unravel the thermal conducting property of h-BN glass, an infrared camera was employed to map out the temperature distribution, where a hot spot was created at the center of the sample by a focused infrared laser beam (1450 nm). The experimental setup is illustrated in Figure 4d, featured by a fixed laser power of 850 mW cm^{-3} and a current density of 1.71 A. As for the bare glass sample, the temperature at the hot spot is ≈50 °C and falls down to only ≈33 °C at the sample edge, due to the limited heat spreading ability of pure glass (blue line in Figure 4e). Evidently, the temperature spike is reduced to ≈48 °C on the thick layer h-BN/quartz glass owing to the enhanced heat

ADVANCED
SCIENCE NEWS

www.advancedsciencenews.com

ADVANCED
MATERIALS
INTERFACES

www.advmatinterfaces.de

spreading effect (red line in Figure 4e). Altogether, the temperature variation within the entire h-BN coated quartz glass is reduced to ≈10 °C (Figure 4f), which is much smaller than that without h-BN coating (≈17 °C, Figure 4h). Hereby, the direct h-BN-coating on glass can substantially improve the thermal performance of adiabatic glass.

The directly grown, transparent, thermal conductive h-BN/ sapphire glass was specifically served as an ideal substrate for the van-der-Waals epitaxial growth of AlN, a fundamental material for developing high-efficiency AlGaN-based DUV-LEDs. Such a growth design was inspired by the fact that both AlN and h-BN are III-nitride materials with similar honeycomb structures. Nevertheless, the nucleation and epitaxial growth of nitride materials directly on the dangling bond free surface of h-BN was still quite challenging.[35] Herein, the as-grown h-BN/ sapphire sample was pretreated by O_2 plasma (80 W, 3 min) to facilitate the nucleation of AlN. Subsequently, AlN epilayer with a thickness of ≈1.3 µm was grown on top of h-BN by virtue of a two-step metal–organic chemical vapor deposition (MOCVD) method, with the experimental details described in the Experimental Section. The h-BN layer remained at the interface after the plasma treatment and AlN growth processes, as evidenced by the XPS analysis shown in Figure S10 (Supporting Information).

The surface morphology and crystalline quality of the AlN epilayer were then evaluated by various surface or interface sensitive characterization methods. The AFM image in **Figure 5**a shows a smooth surface of the epitaxial AlN film featured by well-defined steps and terraces, reflecting the stepflow growth mode of AlN materials on h-BN/sapphires.[36] The

root-mean-square (RMS) roughness in the 5×5 µm^2 area is only ≈0.16 nm, corresponding to an atomic level fluctuation. Furthermore, the cross-sectional HRTEM image in Figure 5b reveals the relative high crystal quality of the AlN layers, as well as the interface of the h-BN buffer layer. The ω-scan X-ray rocking curves (XRCs) of (0002) and (10-12) reflections were also acquired to evaluate the dislocation density in AlN,[37] as shown in Figure 5c and Figure S11 (Supporting Information). The full width at half maximum (FWHM) values for the XRCs of AlN films grown on h-BN/sapphire are found to be 127 and 1099 arcsec for (0002) and (10-12) reflections, respectively. Accordingly, the screw dislocation density and the edge dislocation density were calculated to be 3.51×10^7 and 1.45×10^{10} cm^{-2}, respectively, which is comparable with those of directly grown AlN on sapphire by a similar MOCVD route (≈10^7 and 10^{10} cm^{-2}, respectively).[38]

It is noted that, through a conventional epitaxial growth route, compressive stress in AlN is normally unavoidable due to the large lattice mismatch and thermal expansion coefficient mismatch between the AlN epilayer and the c-plane sapphire substrate.[39] The stress would degrade the device performance of DUV-LEDs fabricated on the AlN template, resulting in severe cracks and electric leakage issues. By employing h-BN/ sapphire as the epitaxial substrate, the direct heteroepitaxial interface changed into vdW–epitaxial interface, leading to significantly reduced strain in the epitaxial AlN. Generally, the in-plane stress (σ_a) of AlN can be estimated by the E_2(high) Raman peak by using $\sigma_a = k^{-1}\triangle\omega[E_2(\text{high})]$ equation, where $\triangle\omega[E_2(\text{high})]$ is the strain-induced Raman frequency shift for the E_2(high) mode. For the stress-free AlN film, the E_2(high)
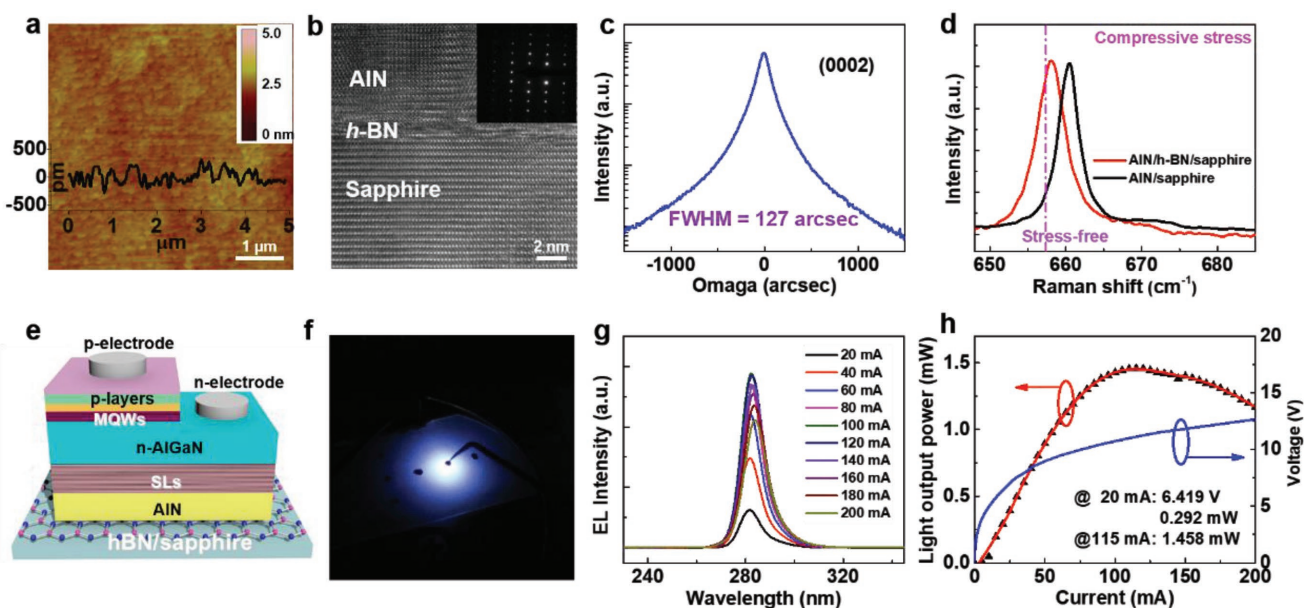
Figure 5. Applications of as-grown h-BN glass in DUV-LEDs. a) AFM image of the AlN epilayer grown on h-BN/sapphire, with the corresponding line profile shown as insets. b) Cross-sectional HRTEM image of the AlN/h-BN/sapphire structures (inset: SAED pattern of epitaxial AlN). c) X-ray rocking curve from AlN epilayer on-axis (0002), showing an FWHM of 127 arcsec. d) Raman spectra of the E_2 (high) peaks of AlN/h-BN/sapphire (red line) and AlN/sapphire (black line), respectively. e) Schematic diagram of the AlGaN-based DUV-LED structure fabricated on h-BN/sapphire. f) Photograph of the electroluminescence from the DUV-LED wafer before the tape-out process. g) EL spectra of the DUV-LEDs measured by varying the injection current from 20 to 200 mA with an interval of 20 mA. h) Light output power (red line) and the I–V characteristic curve (blue line) of the DUV-LEDs plotted as a function of injection current.

**ADVANCED
SCIENCE NEWS**

www.advancedsciencenews.com

**ADVANCED
MATERIALS
INTERFACES**

www.advmatinterfaces.de

Raman peak should be located at ≈657.4 cm^{-1} and the Raman stress factor k is -6.3 cm^{-1} GPa^{-1}.[40,41]

In the current synthetic route, the E_2(high) Raman peak of AlN directly synthesized on h-BN is centered at 658 cm^{-1} (Figure 5d), corresponding to a compressive stress of ≈0.095 GPa, much less than that of AlN directly grown on sapphire.[42] Moreover, the FWHM value of the E_2(high) Raman peak is only 4.37 cm^{-1}, further indicating the relative high crystal quality of AlN films synthesized on h-BN/sapphire.[41] It can be inferred that, the h-BN buffer layer serves as a perfect stress-releasing layer for the epitaxial growth of high-quality AlN films.

The AlGaN-based DUV-LEDs structure (schematically shown in Figure 5e) was accordingly fabricated on the as-grown AlN/h-BN/sapphire template (see the Experimental Section for more details). Room-temperature electroluminescence (EL) measurements (Figure 5f) were then carried out on the DUV-LEDs using the calibrated integrating-sphere system. Figure 5g shows the EL spectra of the DUV-LED structure with the injected current (I) varied up to 200 mA with an interval of 20 mA, respectively, showing characteristics of deep-UV emissions. Moreover, the peak wavelengths of the EL spectra were slightly redshifted from 281.4 nm (20 mA) to 283.8 nm (200 mA) (Figure S12, Supporting Information), due to the thermal induced bandgap narrowing of AlGaN-based multiple quantum well (MQWs) under the high current injection. The current–voltage (I–V) and current–output (I–L) characteristics of the as-achieved DUV-LEDs (Figure 5h) presented a maximal light output power (IOP) of 1.458 mW at the injection current of 115 mA. Notably, the highly transparent h-BN film may not affect the light extraction efficiency of DUV-LEDs, considering its absorption edge at ≈200 nm. However, the absorption edge of graphene overlaps with the light emission wavelength of the DUV-LEDs (≈280 nm), which should lead to decreased light output power of the devices. Altogether, the DUV-LEDs fabricated on h-BN glass have exhibited desirable device performances, which is promising for the development of stress-free, durable LEDs for the next-generation solid-state lighting. Additionally, the facile release and transfer of the LED devices onto large-area, flexible substrates with thick h-BN films are also intriguing, which is an ongoing effort in our lab.

To sum up, we have developed a catalyst-free LPCVD approach for the direct growth of large-area, high-quality, thickness-tunable h-BN films on high-temperature-resistant solid glass. The resultant h-BN glass are featured with fascinating optical transparency, hydrophobic surface, high thermal conductivity, etc., making it readily applicable as perfect substrates for the epitaxial growth of AlN functional layers. High-performance AlGaN-based DUV-LED devices were also realized on h-BN glass, benefited from the much released interfacial stress built upon the weak vdW interaction of AlN/h-BN, as well as the perfect thermal conductivity of the h-BN template. This work hereby sheds light on the scalable production of a new type hybrid of h-BN glass possessing versatile application prospects, from daily-life applications, optoelectronic devices to energy-related applications.

Experimental Section

LPCVD Growth of h-BN Films on Quartz or Sapphire Glass: In a typical procedure, quartz glass and sapphire glass were thoroughly cleaned with deionized water, acetone, and ethanol before being loaded into the quartz tube inside a three-zone furnace. The CVD system was pumped with a base pressure of 0.2 Pa and then inflated with 50 sccm H$_2$ and 50 sccm Ar (100 H$_2$ and 150 Ar for the case of 3 in. tube furnace) as carrier gases. The BH$_3$-NH$_3$ precursor was placed in a quartz cell connected to the CVD growth tube, where a program-controlled heating belt was wrapped around to aid the sublimation at a precursor evaporation temperature (T_p) range of 75–90 °C. The glass samples were heated to 1100 °C and exposed to evaporated BH$_3$-NH$_3$ precursors, which decomposed into borazine, hydrogen, and polyiminoborane. The thicknesses of h-BN samples were controlled by varying the growth time and evaporation temperature of BH$_3$-NH$_3$ precursors. After growth, the samples were cooled down to room temperature under H$_2$ and Ar flows.

DUV-LED Device Fabrications: The as-grown h-BN/sapphire sample was treated by O$_2$ plasma under 80 W power for 3 min to assist the nucleation of AlN. The AlN and AlGaN-based DUV-LED structures were grown on the h-BN/sapphire substrate by MOCVD under a pressure of 50 torr, with hydrogen as carrier gas, ammonia as gaseous supply for N, trimethylaluminum (TMAl) and trimethylgallium (TMGa) as metal–organic precursor for Al and Ga. For n-type and p-type doping, silane (SiH$_4$) and bis(cyclopentadienyl)magnesium (Cp$_2$Mg) were introduced, respectively. The AlN epilayer was grown with an optimized two-step growth process, where a low-temperature (LT) AlN layer was first deposited at 860 °C for 5 min, followed with a high-temperature (HT) AlN layer grown at 1200 °C for 1 h with a V/III ratio of 500. Subsequently, an AlGaN-based DUV-LED structure was grown on the AlN/h-BN/sapphire template, including 20-period AlN/Al$_{0.7}$Ga$_{0.3}$N superlattices (SLs), a 2 μm n-Al$_{0.55}$Ga$_{0.45}$N layer, 5-period Al$_{0.5}$Ga$_{0.5}$N/Al$_{0.4}$Ga$_{0.6}$N multiple quantum wells (MQWs) and p-type layers (a 30-nm p-Al$_{0.65}$Ga$_{0.35}$N electron-blocking layer, a 50-nm p-AlGaN cladding layer, and a 100 nm p-GaN contact layer). The p-type layers were annealed in the reactor at 800 °C in flowing N$_2$ gas for 20 min to activate the Mg acceptors. The DUV-LED devices with a die size of 500 μm × 500 μm were fabricated by standard LED processes of photolithography, inductively coupled plasma (ICP) etching, e-beam evaporation, etc. A Ti/Al/Ti/Au metal stack was deposited on the exposed n-AlGaN as the n-type contact, and a Ni/Au stack was used as the p-type contact. At last, the DUV-LED chips were flip-chip bonded onto ceramic submounts coated with gold for light-output testing.

Characterizations: Characterizations were performed with scanning electron microscopy (SEM) (Hitachi S4800), AFM (Veeco Nanoscope IIIa, tapping mode), Raman (Horiba, LabRAM HR-800, 514.5 nm, 2.41 eV; home-built Raman system composed of Princeton SP2500 spectrometer and Spectra-Physics Mai Tai Laser), TEM (FEI Titan Themis G2, acceleration voltage 30–300 kV), XPS (Kratos Analytical Axis-Ultra spectrometer using a monochromatic Al Kα X-ray source), UV–vis spectroscopy (Perkin–Elmer Lambda 950 spectrophotometer), contact angle system (DataPhysics, OCA20), IR-camera (FLUKE Ti 10 Infrared Camera), X-ray diffraction (Bede D1, 40 kV, 36 mA). The EL spectra and LOP of the DUV-LEDs were achieved by EVERFINE HAAS-2000 high-accuracy array spectroradiometer with a calibrated integrating sphere. The current–voltage (I–V) characteristics of the devices were measured by Keithley 2420.

Supporting Information

Supporting Information is available from the Wiley Online Library or from the author.

Acknowledgements

[1] K. Watanabe, T. Taniguchi, H. Kanda, *Nat. Mater.* **2004**, *3*, 404.

[2] Y. Lin, J. W. Connell, *Nanoscale* **2012**, *4*, 6908.

[3] S. M. Kim, A. Hsu, M. H. Park, S. H. Chae, S. J. Yun, J. S. Lee, D. H. Cho, W. J. Fang, C. Lee, T. Palacios, M. Dresselhaus, K. K. Kim, Y. H. Lee, J. Kong, *Nat. Commun.* **2015**, *6*, 8662.

[4] Z. Liu, Y. J. Gong, W. Zhou, L. L. Ma, J. J. Yu, J. C. Idrobo, J. Jung, A. H. MacDonald, R. Vajtai, J. Lou, P. M. Ajayan, *Nat. Commun.* **2013**, *4*, 2541.

[5] J. Xue, J. Sanchez-Yamagishi, D. Bulmash, P. Jacquod, A. Deshpande, K. Watanabe, T. Taniguchi, P. Jarillo-Herrero, B. J. LeRoy, *Nat. Mater.* **2011**, *10*, 282.

[6] L. H. Li, J. Cervenka, K. Watanabe, T. Taniguchi, Y. Chen, *ACS Nano* **2014**, *8*, 1457.

[7] R. Decker, Y. Wang, V. W. Brar, W. Regan, H. Z. Tsai, Q. Wu, W. Gannett, A. Zettl, M. F. Crommie, *Nano Lett.* **2011**, *11*, 2291.

[8] C. Zhi, Y. Bando, C. Tang, H. Kuwahara, D. Golberg, *Adv. Mater.* **2009**, *21*, 2889.

[9] H. L. Zhu, Y. Y. Li, Z. Q. Fang, J. J. Xu, F. Y. Cao, J. Y. Wan, C. Preston, B. Yang, L. B. Hu, *ACS Nano* **2014**, *8*, 3606.

[10] C. R. Dean, A. F. Young, I. Meric, C. Lee, L. Wang, S. Sorgenfrei, K. Watanabe, T. Taniguchi, P. Kim, K. L. Shepard, J. Hone, *Nat. Nanotechnol.* **2010**, *5*, 722.

[11] W. Yang, G. R. Chen, Z. W. Shi, C. C. Liu, L. C. Zhang, G. B. Xie, M. Cheng, D. M. Wang, R. Yang, D. X. Shi, K. Watanabe, T. Taniguchi, Y. G. Yao, Y. B. Zhang, G. Y. Zhang, *Nat. Mater.* **2013**, *12*, 792.

[12] C. R. Dean, L. Wang, P. Maher, C. Forsythe, F. Ghahari, Y. Gao, J. Katoch, M. Ishigami, P. Moon, M. Koshino, T. Taniguchi, K. Watanabe, K. L. Shepard, J. Hone, P. Kim, *Nature* **2013**, *497*, 598.

[13] B. Hunt, J. D. Sanchez-Yamagishi, A. F. Young, M. Yankowitz, B. J. LeRoy, K. Watanabe, T. Taniguchi, P. Moon, M. Koshino, P. Jarillo-Herrero, R. C. Ashoori, *Science* **2013**, *340*, 1427.

[14] L. Song, L. J. Ci, H. Lu, P. B. Sorokin, C. H. Jin, J. Ni, A. G. Kvashnin, D. G. Kvashnin, J. Lou, B. I. Yakobson, P. M. Ajayan, *Nano Lett.* **2010**, *10*, 3209.

[15] Y. Shi, C. Hamsen, X. Jia, K. K. Kim, A. Reina, M. Hofmann, A. L. Hsu, K. Zhang, H. Li, Z.-Y. Juang, M. S. Dresselhaus, L.-J. Li, J. Kong, *Nano Lett.* **2010**, *10*, 4134.

[16] Y. Gao, W. Ren, T. Ma, Z. Liu, Y. Zhang, W.-B. Liu, L.-P. Ma, X. Ma, H.-M. Cheng, *ACS Nano* **2013**, *7*, 5199.

[17] G. Lu, T. Wu, Q. Yuan, H. Wang, H. Wang, F. Ding, X. Xie, M. Jiang, *Nat. Commun.* **2015**, *6*, 6160.

[18] X. Li, Y. Zhu, W. Cai, M. Borysiak, B. Han, D. Chen, R. D. Piner, L. Colombo, R. S. Ruoff, *Nano Lett.* **2009**, *9*, 4359.

[19] S. Bae, H. Kim, Y. Lee, X. F. Xu, J. S. Park, Y. Zheng, J. Balakrishnan, T. Lei, H. R. Kim, Y. I. Song, Y. J. Kim, K. S. Kim, B. Ozyilmaz, J. H. Ahn, B. H. Hong, S. Iijima, *Nat. Nanotechnol.* **2010**, *5*, 574.

[20] J. Y. Sun, Y. B. Chen, M. K. Priydarshi, Z. Chen, A. Bachmatiuk, Z. Y. Zou, Z. L. Chen, X. J. Song, Y. F. Gao, M. H. Rummeli, Y. F. Zhang, Z. F. Liu, *Nano Lett.* **2015**, *15*, 5846.

[21] Y. B. Chen, J. Y. Sun, J. F. Gao, F. Du, Q. Han, Y. F. Nie, Z. Chen, A. Bachmatiuk, M. K. Priydarshi, D. L. Ma, X. J. Song, X. S. Wu, C. Y. Xiong, M. H. Rummeli, F. Ding, Y. F. Zhang, Z. F. Liu, *Adv. Mater.* **2015**, *27*, 7839.

[22] X.-D. Chen, Z. Chen, W.-S. Jiang, C. Zhang, J. Sun, H. Wang, W. Xin, L. Lin, M. K. Priydarshi, H. Yang, Z.-B. Liu, J.-G. Tian, Y. Zhang, Y. Zhang, Z. Liu, *Adv. Mater.* **2017**, *29*, 1603428.

[23] S. Behura, P. Nguyen, S. W. Che, R. Debbarma, V. Berry, *J. Am. Chem. Soc.* **2015**, *137*, 13060.

[24] A. R. Jang, S. Hong, C. Hyun, S. I. Yoon, G. Kim, H. Y. Jeong, T. J. Shin, S. O. Park, K. Wong, S. K. Kwak, N. Park, K. Yu, E. Choi, A. Mishchenko, F. Withers, K. S. Novoselov, H. Lim, H. S. Shin, *Nano Lett.* **2016**, *16*, 3360.

[25] Y. Kobayashi, C.-L. Tsai, T. Akasaka, *Phys. Status Solidi C* **2010**, *7*, 1906.

[26] Y. Kobayashi, T. Akasaka, *J. Cryst. Growth* **2008**, *310*, 5044.

[27] Y. Kobayashi, K. Kumakura, T. Akasaka, T. Makimoto, *Nature* **2012**, *484*, 223.

[28] J. H. Choi, J. Kim, H. Yoo, J. Liu, S. Kim, C.-W. Baik, C.-R. Cho, J. G. Kang, M. Kim, P. V. Braun, S. Hwang, T.-S. Jung, *Adv. Opt. Mater.* **2016**, *4*, 505.

[29] N. Han, T. V. Cuong, M. Han, B. D. Ryu, S. Chandramohan, J. B. Park, J. H. Kang, Y. J. Park, K. B. Ko, H. Y. Kim, H. K. Kim, J. H. Ryu, Y. S. Katharria, C. J. Choi, C. H. Hong, *Nat. Commun.* **2013**, *4*, 1452.

[30] K. Chung, H. Oh, J. Jo, K. Lee, M. Kim, G. C. Yi, *NPG Asia Mater.* **2017**, *9*, e410.

[31] Y. Li, Y. Rao, K. F. Mak, Y. You, S. Wang, C. R. Dean, T. F. Heinz, *Nano Lett.* **2013**, *13*, 3329.

[32] R. R. Nair, P. Blake, A. N. Grigorenko, K. S. Novoselov, T. J. Booth, T. Stauber, N. M. R. Peres, A. K. Geim, *Science* **2008**, *320*, 1308.

[33] H. Li, X. C. Zeng, *ACS Nano* **2012**, *6*, 2401.

[34] N. Giovambattista, P. G. Debenedetti, P. J. Rossky, *J. Phys. Chem. B* **2007**, *111*, 9581.

[35] Q. Wu, J. Yan, L. Zhang, X. Chen, T. Wei, Y. Li, Z. Liu, X. Wei, Y. Zhang, J. Wang, J. Li, *CrystEngComm* **2017**, *19*, 5849.

[36] W. K. Luo, L. Li, Z. H. Li, Q. K. Yang, D. G. Zhang, X. Dong, D. Q. Peng, L. Pan, C. H. Li, B. Liu, R. Zhong, *J. Alloys Compd.* **2017**, *697*, 262.

[37] B. N. Pantha, R. Dahal, M. L. Nakarmi, N. Nepal, J. Li, J. Y. Lin, H. X. Jiang, Q. S. Paduano, D. Weyburne, *Appl. Phys. Lett.* **2007**, *90*, 241101.

[38] K. Ding, V. Avrutin, Ü. Özgür, H. Morkoç, *Crystals* **2017**, *7*, 300.

[39] X. Rong, X. Wang, G. Chen, J. Pan, P. Wang, H. Liu, F. Xu, P. Tan, B. Shen, *Superlattices Microstruct.* **2016**, *93*, 27.

[40] T. Prokofyeva, M. Seon, J. Vanbuskirk, M. Holtz, S. A. Nikishin, N. N. Faleev, H. Temkin, S. Zollner, *Phys. Rev. B* **2001**, *63*, 125313.

[41] J. D. Greenlee, B. Gunning, B. N. Feigelson, T. J. Anderson, A. D. Koehler, K. D. Hobart, F. J. Kub, W. A. Doolittle, *Electron. Mater. Lett.* **2016**, *12*, 133.

[42] P. Dong, J. C. Yan, Y. Zhang, J. X. Wang, J. P. Zeng, C. Geng, P. P. Cong, L. L. Sun, T. B. Wei, L. X. Zhao, Q. F. Yan, C. G. He, Z. X. Qin, J. M. Li, *J. Cryst. Growth* **2014**, *395*, 9.